等离子喷涂双层热障涂层沉积过程的数值模拟

侯平均，　王汉功，　汪刘应，　袁晓静
（第二炮兵工程学院 501 室，西安　710025）

侯平均

摘　要：运用 ANSYS10.0 有限元分析软件对等离子喷涂典型双层热障涂层沉积过程的温度和应力变化过程进行了数值模拟. 结果表明，喷涂过程中，基体背面温度呈台阶状上升，涂层颗粒的温度大幅度周期波动，涂层颗粒的应力随之大幅度周期波动；喷涂结束后，涂层内的残余应力趋于稳定，x 方向的最大拉应力存在于陶瓷层与粘结层结合面的边缘；最大 y 方向拉应力和层间应力都存在于陶瓷层和粘结层的结合面上. 涂层的结合面边缘是应力集中部位，结合面的中部应力分布均匀. 陶瓷层表面 x 方向的最大拉应力为 423.7 MPa.

关键词：数值模拟；等离子喷涂；热障涂层；温度场；残余应力
中图分类号：TG148　　文献标识码：A　　文章编号：0253－360X(2009)11－0097－04

0　序　　言

在等离子喷涂制备热障涂层过程中，基体与涂层将随着温度的改变而变形，由于涂层与基体线膨胀系数(CTE)不匹配，涂层与基体中将产生残余应力，这可能会引起涂层与基体的剥离[1]. 由于热喷涂涂层所具有的特性，加上各种测试方法本身的特点和有限的测试条件，采用各种测试方法欲获得涂层残余应力的准确值仍存在一定的难度. 现阶段，计算机和各种模拟工具的发展，使得研究涂层沉积过程产生的残余应力成为可能[2,3]. 程世杰等人[4]、Ng 等人[5] 应用有限元分析软件模拟了等离子喷涂过程中涂层中产生的残余应力，但都是采用逐层分析的方法，与大面积涂层制备有差别.

文中运用有限元分析软件 ANSYS10.0，采用单元“生死”技术，通过逐个“激活”涂层单元来模拟等离子喷涂双层 ZrO_2/NiCoCrAlY 热障涂层的沉积过程，计算此过程中涂层的温度和应力，为优化制备热障涂层工艺参数提供参考依据.

1　模型建立

1.1　几何模型

模拟在厚度为 20 mm 的不锈钢基体上制备双层热障涂层的粘结层和陶瓷层厚度均为 0.3 mm. 每种涂层分别再分为三薄层(薄层的厚度均为 0.1 mm)，模拟喷涂每种涂层按照“左—右，右—左”的顺序连续“激活”相邻涂层单元方式进行. 几何模型及有限元网格划分如图 1 所示.

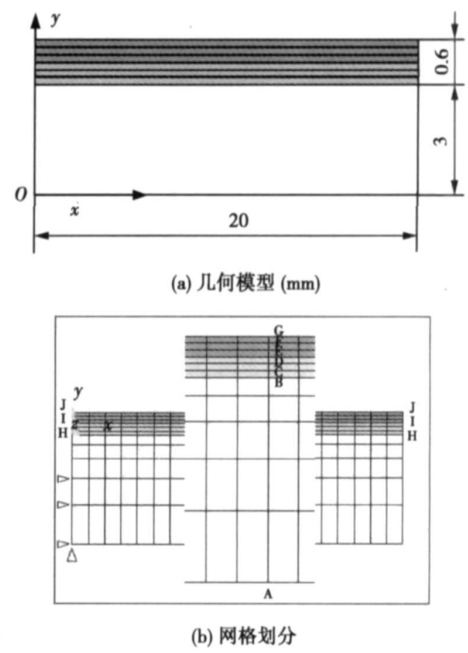

图 1　热障涂层模型

Fig. 1　Models of TBCs for finite element analysis

1.2　涂层材料及基体物理参数

模拟等离子喷涂制备典型双层热障涂层的涂层材料及基体的物理参数如表 1 所示[5,6].

收稿日期：2008－12－18

表 1 涂层与基体的物理参数

Table 1 Properties of coatings and substrate

材料	温度 T/℃	密度 ρ/(kg·m^{-3})	弹性模量 E/GPa	屈服强度 R_{eL}/MPa	切变模量 G/MPa	泊松比 μ	线膨胀系数 α_l/(10^{-6}K^{-1})	热导率 λ/(W·m^{-1}·K^{-1})	比热容 c/(J·kg^{-1}·K^{-1})
ZrO_2	25	5 700	53			0.230	9.1	0.55	500
	400						10.2	0.61	576
	800						10.9	0.65	637
NiCoCrAlY	25	7 320	225	300	688	0.300	11.6	4.3	501
	400		186				14.0	6.4	592
	800		147				16.0	10.2	781
1Cr18Ni9Ti	25	7 900	198	1 400	20 600	0.243	—	—	502
	200		189	—	—	0.250	17.0	17.6	
	400		174	—	—	—	17.5	20.5	
	600		157	1 000	17 000	—	18.2	23.5	
	800		—	—	—	—	—	26.4	
	1 000		—	500	9 000	—	—	—	
	2 000		—	7	100	—	—	—	

2 有限元计算

在分析中做以下几点假设:(1) 整个涂层系统(陶瓷层、粘结层和基体)没有缺陷. (2) 基体和粘结层材料服从双线性随动强化模型,而且材料为各向同性. (3) 陶瓷层、粘结层和基体之间的界面为光滑界面,不考虑界面粗糙度的影响,在界面处不产生相对滑动. (4)在热分析过程中,只考虑试样表面与空气对流传热,不考虑辐射传热的影响.

2.1 边界条件

喷涂过程中对流载荷条件[5] 如图 2 所示. 其中, h_b=8 W/(m^2·K), T_b=30 ℃; h_r=20 W/(m^2·K), T_r=127 ℃; h_i=320 W/(m^2·K), T_i=700 ℃(喷涂粘结层), T_i=800 ℃(喷涂陶瓷层). 粘结层和陶瓷层单元初始温度分别为它们的熔点:1 400, 2 205 ℃. 它们的结晶潜热分别为 2.196×10^9 J/m^3 和 4.286×10^9 J/m^3. 在喷涂结束以后,试样的四周加载 h_b=8 W/(m^2·K), T_b=30 ℃的对流载荷,自然冷却 1 000 s.

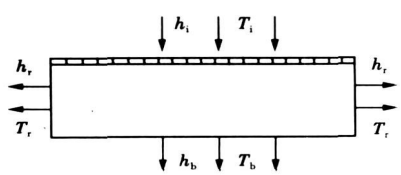

图 2 喷涂过程中对流载荷条件

Fig. 2 Convection conditions of spraying process

2.2 计算过程

采用热—结构直接耦合单元 PLANE13 进行温度和残余应力计算. 模型的网格划分如图 1 所示. 计算时,首先加载边界条件,应用 APDL 命令流控制计算过程,先将涂层单元全部"杀死",然后按照"从左到右,再从右到左"的顺序逐一"激活"涂层单元,进行分析计算.

3 数值模拟结果与分析

3.1 涂层沉积过程中的温度变化

图 2 为喷涂最后一层陶瓷涂层时,加载第 461 步温度载荷后的温度场云图. 此时陶瓷颗粒的温度为 2 478 K(2 205 ℃),陶瓷颗粒处于熔融状态,与之接触的单元吸收该颗粒的热量温度升高,温度场呈"扇形"分布. 基体表面沉积 5 层涂层后,基体的最低温度也从 27 ℃上升到 249 ℃,随着喷涂的进行基体温度继续升高,喷涂结束时达到最高值.

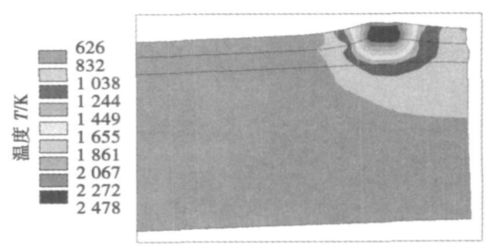

图 3 第 461 步温度场云图

Fig. 3 Temperature contour of 461 step

在基体背面和每一层涂层表面的中间位置各选取一个节点,节点位置见图 1. 图 4a 为 A 点的温度

随时间变化曲线，可以看出，随着喷涂的进行，A 点的温度呈阶梯状升高．A 点的最高温度为 581 ℃．图 4b，c 分别为节点 D 和 G 的温度随时间变化曲线．涂层单元被“激活”时（也就是涂层颗粒沉积时），单元上的节点温度达到最高．节点 D 是第 3 层粘结层表面上的节点，后续 3 层陶瓷层沉积到此位置时，该点温度出现了 3 次峰值，但随着涂层的增厚，后续沉积涂层对其温度的影响也逐渐减弱．涂层颗粒在喷涂过程中经历多次快速升温和快速降温的热冲击作用，这会使涂层中产生较大的应力．喷涂结束后经过 1 000 s 冷却，涂层和基体的温度基本均匀达到室温．

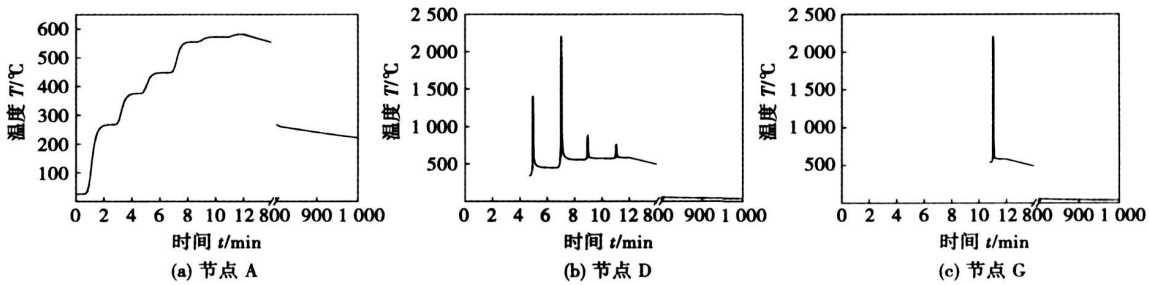

图 4　不同节点的温度随时间变化曲线

Fig 4　Temperature curves of nodes

3.2　涂层沉积过程中的应力分析

图 5 为节点 D 的应力随时间变化曲线．D 点 5 s 以前的应力为 0，该点所在的单元在 5 s 之前未被“激活”，也就是涂层颗粒还没有沉积．之后，该点的应力在喷涂过程中剧烈波动，喷涂结束后应力逐步稳定．D 点的 σ_x（x 方向应力）波动幅度较大（图 5a），这是因为 D 点经历了 4 次被快速加热和快速冷却过程，该单元在快速膨胀和收缩过程中产生了较大的 x 方向应力．喷涂结束后，经过自然冷却，D 点的 σ_x 逐渐稳定约为 80 MPa 的拉应力．D 点的 σ_y（y 方向应力）和 σ_{xy}（层间应力）也存在一定幅度的拉应力和压应力波动（图 5b，c），但最后都变为较小的压应力，这是因为 D 点 y 方向和层间的温度梯度很小．

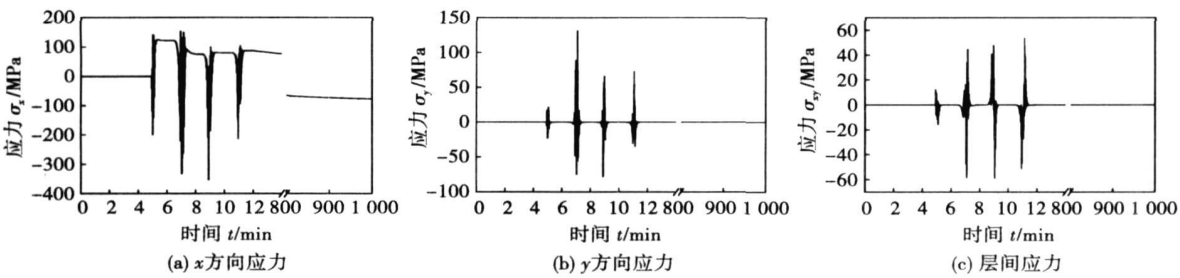

图 5　节点 D 的应力随时间变化曲线

Fig 5　Stress curves of node D

图 6a 为试样自然冷却到室温后 σ_x 的分布，最大拉应力为 466 MPa，存在于陶瓷层和粘结层的结合面的边缘，这是因为陶瓷层快速冷却收缩时会对粘结层产生拉伸作用．陶瓷层表面也存在较大拉应力，这是因为粘结层的整体膨胀对陶瓷层产生拉伸作用，另外，陶瓷层表面在冷却收缩过程中也会产生相反方向拉应力，这是造成陶瓷层表面存在大量微裂纹的原因．x 方向最大压应力为 258 MPa，存在于基体与粘结层的结合界面处，这是由于喷涂时粘结层收缩造成的．图 6b 为试样自然冷却到室温后 σ_y 的分布，最大拉应力为 161 MPa，存在于陶瓷层与粘结层的结合面上．这是由于陶瓷层与粘结层的线膨胀系数不同，降温收缩时粘结层收缩量大，在 y 方向上对陶瓷层产生了较大的拉应力．造成陶瓷层与粘结层的结合强度较低，所以在热震过程中陶瓷层最容易剥落．图 6c 为试样自然冷却到室温后 σ_{xy} 的

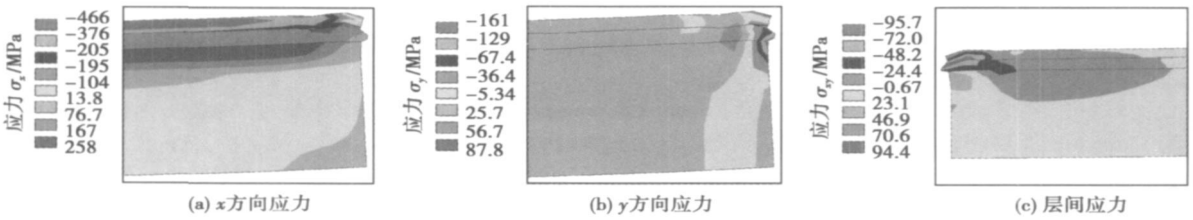

图 6 试样冷却至室温后涂层残余应力分布

Fig 6 Residual stress contours at room temperature

分布, 其中最大层间拉应力为 95.7 MPa, 也存在于陶瓷层和粘结层的结合面上.

结合面是应力集中部位, 在有限元模型上定义路径:H—H、I—I 和 J—J(图 1), 分别代表粘结层与基体结合面、陶瓷层与粘结层结合面和陶瓷层表面. 喷涂结束时, 界面上的残余应力分布如图 7 所示. 涂层结合面边缘处是应力集中和应力急剧变化的部位, 这是因为该部位材料的热力学性能出现突变, 传热条件复杂, 另外喷涂过程中该部位在较短时间内经历了两次快速升温和降温过程, 温度剧烈变化造成应力集中. H—H 界面上, x 方向主要存在压应力(图 7a), 最大值为 221.6 MPa; 在涂层边缘 y 方向上的拉应力最大, 最大值为 174.0 MPa; 涂层边缘的层间应力主要为拉应力. I—I 界面上, 三种应力在 x=0 附近达到最大拉应力(图 7b), 在 x=2.0 mm 附近达到最大压应力; 在试样中部 x 方向的拉应力约为 80 MPa. J—J 表面 x 方向上存在较大拉应力(图 7c), 其中试样中部较大范围存在拉应力, 最大值为 423.7 MPa. Ng 等人[5] 采用逐层沉积的方法模拟计算出涂层冷却到室温时, 陶瓷层表面中部的 x 方向上拉应力为 411 MPa. 这个数值与文献[7] 给出的值也比较接近.

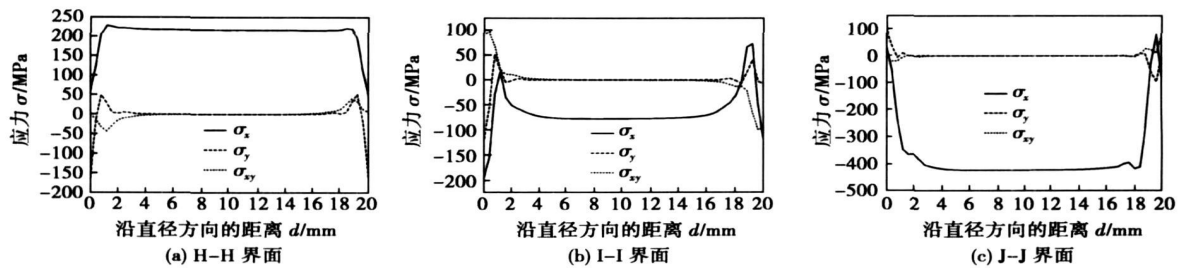

图 7 残余应力沿界面的变化曲线

Fig 7 Residual stress curves along interfaces

4 结 论

(1) 数值模拟涂层沉积过程中, 基体背面温度呈台阶状上升, 最高温度为 581 ℃; 涂层颗粒的温度大幅度周期波动.

(2) 喷涂过程中陶瓷层与粘结层结合面上节点 D 的 x 方向应力大幅度周期波动, 喷涂结束后, 应力逐渐减小为 80 MPa 的拉应力; y 方向应力和层间应力在喷涂过程中小幅度波动.

(3) 喷涂结束后, x 方向最大拉应力为 466 MPa, 存在于陶瓷层与粘结层结合面的边缘; 最大 y 方向拉应力和层间应力都存在于陶瓷层和粘结层的结合面处, 分别为 161, 95.7 MPa.

(4) 涂层的结合面边缘处是应力集中部位, 结合面的中间部分应力均匀. 粘结层与基体的结合面上, x 方向最大压应力为 221.6 MPa; y 方向最大拉应力为 174.0 MPa. 陶瓷层表面的 x 方向最大拉应力为 423.7 MPa.

参考文献:

[1] Zhang Xiancheng, Gong Jianning, Tu Shandong. Effects of condition and material properties on the residual stress in plasma spraying[J]. Journal Materials Science and Technology, 2004, 20(2): 149—153.

[下转第 104 页]

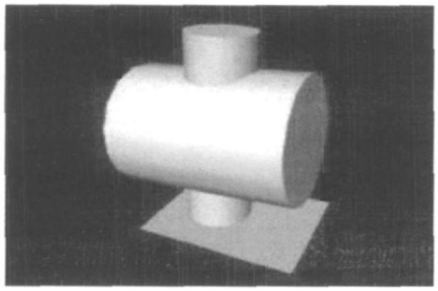

图 5 重建的马鞍形工件三维模型

Fig. 5 Reconstructed 3D model of saddle workpiece

4 结 论

(1) 改进的视差图分割算法在法线计算和区域增长之后,再进行区域合并,通过边界探测和合并曲面步骤,能够将属于同一曲面的区域重新合并到一起. 较好地完成了含有圆柱面的视差图的分割,且避免了通用算法计算的复杂性和鲁棒性问题.

(2) 通过立体视觉系统对马鞍形工件进行三维重建的结果说明,该算法可以用于实际焊接工件的视差图分割,其三维重建结果满足遥控焊接初始运动规划的精度要求.

参考文献:

[1] Johnson A, Leger P, Hoffman R, *et al*. 3-D object modeling and recognition for telerobotic manipulation[C] // Proceedings of IEEE Intelligent Robots and Systems, Pittsburgh, USA, 1995: 103—110.

[2] 李金泉. 基于视觉弧焊机器人焊缝空间位置信息获取技术的研究[D]. 哈尔滨: 哈尔滨工业大学, 2003.

[3] Wang Z L, Zhang J, Cai H G. Multibaseline stereo with active illumination and its application in robot welding[J]. China Welding, 2000, 9(2): 152—160.

[4] Liang Z M, Gao H M, Wang Z J, *et al*. 3D reconstruction of welding environment based on spacetime stereo[J]. Lecture Notes in Control and Information Sciences: Robotic Welding, Intelligence and Automation, 2007, 362: 211—218.

[5] Liang Z M, Gao H M, Nie L, *et al*. 3D reconstruction for telerobotic welding[C] // Proceedings of IEEE International Conference on Mechatronics and Automation, Harbin, China, 2007: 475—479.

[6] Hoover A, Jean-Baptiste G, Jiang X, *et al*. An experimental comparison of range image segmentation algorithms[J]. IEEE Transactions on Pattern Analysis and Machine Intelligence, 1996, 18(7): 673—689.

作者简介: 王 军, 男, 1968 年出生, 博士, 副教授, 硕士生导师. 主要从事先进连接技术及焊接过程自动控制方面的教学和科研工作. 发表论文 20 余篇.

Email: hebustwangjun@163.com

[上接第 100 页]

[2] Bengtsson P, Persson C. Modeled and measured residual stresses in plasma sprayed thermal barrier coatings[J]. Surface & Coating Technology, 1997, 191(92): 78—86.

[3] Lugscheider E, Barimani C, Eritt U, *et al*. FE-simulations of temperature and stress field distribution in thermally sprayed coatings due to deposition process[C] // Proceedings of the 15th International Thermal Spray Conference, France, 1998: 367—372.

[4] 程世杰, 高嘉爽, 刘爱国, 等. 聚酰亚胺复合材料等离子喷涂温度场的数值模拟[J]. 焊接学报, 2006, 27(7): 101—104.
Cheng Shijie, Gao Jiashuang, Liu Aiguo, *et al*. Temperature numerical simulation of plasma sprayed polymerized imide coating[J]. Transactions of the China Welding Institution, 2006, 27(7): 101—104.

[5] Ng H W, Gan Z. A finite element analysis technique for predicting as-sprayed residual stresses generated by the plasma spray coating process [J]. Finite Elements in Analysis and Design, 2005, 41: 1235—1254.

[6] 机械工程材料性能手册编委. 机械工程材料性能手册[M]. 北京: 机械工业出版社, 1995.

[7] Evans A G, Mumm D R, Hutchinson J W, *et al*. Mechanisms controlling the durability of thermal barrier coatings[J]. Progress in Materials Science, 2001, 46(5): 505—553.

作者简介: 侯平均, 男, 1974 年出生, 博士研究生, 工程师. 主要从事表面工程方面的研究工作. 发表论文 10 余篇.

Email: bighou@126.com

would seriously impair the properties of the soldered joint is found.

Key words: Zn based alloy; interfacial zone; reaction mechanism; microstructure

Finite element analysis on reliability of lead-free soldered joints for CSP device YE Huan, XUE Songbai, ZHANG Liang, WANG Hui (College of Materials Science and Technology, Nanjing University of Aeronautics and Astronautics, Nanjing 210016, China). p 93—96

Abstract: Finite element method was employed to analyze the reliability of soldered joint in a CSP device. Anand model was used to establish the constitutive equation of Sn3.0Ag0.5Cu solder, the stress behavior of soldered joint was studied. The results indicate that the maximal stress is located at the upper surface of the soldered joint which is under the outermost of chip. The phenomenon of stress relaxation and accumulated enhancement could be observed obviously from the curves of stress and temperature with time cycle. Reliability of soldered joints with three usually-used heights are compared, and the results shows that the 0.35 mm × 0.18 mm one has the best reliability. Moreover, the influence of chip thickness on the reliability of soldered joints are investigated in the last part, the simulation result indicates that the influence is little.

Key words: chip scale package; lead-free soldered joint; reliability; finite element analysis

Numerical simulation on deposition process of duplex thermal barrier coating by plasma spraying HOU Pingjun, WANG Hangong, WANG Liuying, YUAN Xiaojing (501 staff, The Second Artillery Engineering College, Xi'an 710025, China). p 97—100, 104

Abstract: Numerical simulation was performed by finite element analysis (FEA) to investigate the temperature and stress in a typical duplex thermal barrier coating. During the spraying process, the temperature of the back surface of substrate increases step by step, both the temperature and the stress of the coating fluctuate periodically within a wide range. After the deposition, the specimen was cooled to the room temperature slowly. The stresses become constant values, and the maximum radial tensile stress exists at the interface between the ceramic layer and the bonding layer, and the maximum axial and shear stresses exist at the interface, where is the concentrated stress area. The stresses of the middle interfaces are uniform. The maximum tensile stress on the ceramic layer surface is 423.7 MPa.

Key words: numerical simulation; plasma spraying; thermal barrier coatings; temperature field; residual stress

A disparity map segmentation algorithm for 3D reconstruction of weld workpiece WANG Jun[1], LIANG Zhimin[1,2], GAO Hongming[2] (1. School of Materials Science and Technology, Hebei University of Science and Technology, Shijiazhuang 050018, China; 2. State Key Laboratory of Advanced Welding Production Technology, Harbin Institute of Technology, Harbin 150001, China). p 101—104

Abstract: In remote welding, the segmentation of disparity map is an important step to create 3D model of weld workpiece by stereo vision sensor. In this paper, the USF plane range image segmentation algorithm was introduced into disparity map segmentation, and by a region combination step, the revised algorithm can deal with the disparity map containing cylinder surface. The combination step could be divided into boundary detecting and curve region relabeling. During boundary detection, the pixel at the boundary of the segmented region after plane segmentation was recorded. In curve region relabeling, the adjacent regions in the same curved surface were assigned with the same label by comparing the boundary pixels' normal direction and distance between them. A segmented result of disparity map of saddle workpiece is shown to prove the feasibility of the algorithm.

Key words: disparity map segmentation; stereo vision; 3D reconstruction; remote welding.

Integrated life prediction method of ball grid array soldered joint CHEN Ying, KANG Rui (Department of System Engineering of Engineering Technology, Beijing University of Aeronautics & Astronautics, Beijing 100191, China). p 105—108

Abstract: To quickly estimate the soldered joint lifetime of the ball grid array package, the analytical model of the simplified stress distribution was founded and the thermal fatigue lifetime was calculated by the creep lifetime prediction model. When the precise results were needed, the three dimensional finite element model was founded and the stress distribution in soldered joint was calculated by Anand constructive function of ANSYS, then the thermal fatigue lifetime was given by the Darveaux model. The analytical method and the finite element method were integrated to a main program by the secondary development function of ANSYS. With this program, the lifetime of the soldered joint can be quickly estimated or precisely predicted with the packaging and soldered joint dimension, material parameters and the thermal cycle parameters. Results of the case show that the analytical model results are more sensitive to the variation of the parameters, while the analyzed results by finite element model are stable.

Key words: ball grid array package; soldered joint; analytical method; FEA; lifetime predication

Effect of Ti content on microstructure toughness of deposited metal with flux cored wire WANG Zheng[1], GUI Chibin[1], WANG Yuhua[2] (1. College of Naval Architecture & Power, Naval University of Engineering, Wuhan 430033, China; 2. Naval Military Delegation Room of 407 Factory, Luoyang 471039, Henan, China). p 109—112

Abstract: The effects of Ti content on microstructure characteristic of deposited metal with flux cored wire were investigated with different contents of Ti-Fe powder under the protection of CO_2 and Ar + 20% CO_2. The results show that the inclusions in deposited metal are mainly complex oxides composed of MnO-TiO_x-Al_2O_3-SiO_2 in Si-Mn-Ti deoxidized flux cored wire. With the increasing of Ti content in flux cored wire, the content of Ti in the inclusions increases, and most of inclusions are in the range of 0.3 ~ 2.0 μm in diameter, which promote the formation of acicular ferrite, thus those contribute to the increased toughness of deposited metal. Dissociative Ti can improve the intensity and the rigidity of microstructure, but it does worse to the microstructure toughness when too much dissociative Ti gets into the microstructure of deposited metal.

Key words: Ti; deposited metal; inclusion; toughness